Available online at www.sciencedirect.com
SCIENCE DIRECT
Journal of Colloid and Interface Science 297 (2006) 696–704
JOURNAL OF Colloid and Interface Science
www.elsevier.com/locate/jcis

On the mechanisms of dissolution of montroydite [HgO(s)]: Dependence of the dissolution rate on pH, temperature, and stirring rate

Ana Hocsman [a], Susana Di Nezio [b], Laurent Charlet [c], Marcelo Avena [b,*]

[a] *Departamento de Fisicoquímica, Facultad de Ciencias Químicas, Universidad Nacional de Córdoba, Ciudad Universitaria, 5000 Córdoba, Argentina*
[b] *Departamento de Química, Universidad Nacional del Sur, Av. Alem 1253, 8000 Bahía Blanca, Argentina*
[c] *LGIT, University of Grenoble-I, BP 53, F-38041 Grenoble cedex 9, France*

Received 5 October 2005; accepted 11 November 2005

Available online 19 December 2005

Abstract

The dissolution behavior of montroydite (HgO) has been studied using a fully automated system. Dissolution data under equilibrium conditions are in agreement with previously published data and indicate that HgO solubility is relatively high and constant between pH 4 and 10.1 and increases markedly at pH < 4. The dissolution rate also has similar behavior: it is relatively high and constant between pH 4 and 10.1 and increases sharply at pH < 4. The dissolution process obeys a three-dimensional contraction or attrition mechanism. The dissolution rate increases with increasing temperature and stirring rate and is the result of mixed transport and reaction control. The rate of HgO dissolution is considerably higher than that of other divalent metal oxides at low pH. This high rate is due to the ability of Hg(II) to rapidly exchange its ligands. Data suggest that montroydite will only occur in nature in highly contaminated sites and indicate that Hg oxidation products that are formed at the liquid Hg/water interface may dissolve rapidly.

Keywords: Mercury oxide; Dissolution kinetics; Dissolution mechanism; Oxide minerals

1. Introduction

Mercury (Hg) is one of the most toxic elements. Its presence in the environment is the result of its release from several sources, the most important being waste incinerators and crematoria, industrial plants (such as the chloralkali industry), and gold mining activities. In the last two cases, where large amounts of liquid Hg^0 are used, between 55% and 95% of this element is released to the atmosphere as gaseous elemental mercury [1], the rest probably being lost either directly to soil and rivers in metallic liquid form or as dissolved gaseous mercury [2].

Mercury occurs in various chemical forms. Most atmospheric Hg is made up of gaseous elemental mercury (Hg^0). In surface waters and soils it occurs as elemental mercury (soluble Hg^0 or droplets of liquid mercury) and as Hg(II) compounds [1,3]. In highly contaminated sites several mercury minerals have also been detected, especially highly insoluble ones such as cinnabar and metacinnabar (two polymorphs of HgS) and more soluble ones such as montroydite (HgO) [3]. Understanding the chemical properties of these minerals, especially their dissolution behavior, is essential for assessment of the potential bioavailability and environmental impact of mercury.

Although a great deal of mercury is released to the environment as Hg^0, its occurrence as Hg(II) species indicates that Hg^0 oxidation is important. In the gaseous phase, the oxidation reaction has been rather well studied and several possible mechanisms are known for this process [4,5]. In the aqueous phase, dissolved Hg^0 species can be readily oxidized by oxygen in the presence of chloride and bromide [6,7]. Although less explored in the literature, the case of liquid mercury oxidation in aqueous media has been also studied and there are laboratory experiments showing that droplets of liquid mercury are rapidly oxidized by oxygen when placed in water in the presence of chloride or thiol compounds [1,6,8].

* Corresponding author. Fax: +54 291 4595160.
E-mail address: mavena@uns.edu.ar (M. Avena).

0021-9797/$ – see front matter
doi:10.1016/j.jcis.2005.11.020

The mechanism of oxidation and dissolution of mercury droplets is poorly understood so far. Magalhães and Tubino [1] proposed a mechanism where liquid mercury generates dissolved Hg^0, which undergoes oxidation in the aqueous phase and further complexation with chloride ions. They also suggested a different mechanism, where the first step is the oxidation of metallic mercury at the surface of the droplets, with subsequent dissolution of the oxidized element. Their experiments could not differentiate between the two mechanisms. More recently, Amyot et al. [6] have shown that the oxidation of liquid mercury is faster than that of dissolved mercury in oxygenated water containing chloride ions. They also indicated that the liquid Hg^0/solution interface plays a critical role in the process and that oxidation products are formed at the surface of the droplets. Since oxygen is the oxidizing agent, it is likely that oxygen–mercury species, such as Hg(II) oxide or Hg(II) hydroxide, are formed at the surface of liquid mercury during oxidation and that these species are the ones that undergo dissolution. The mechanisms involved in the oxidative dissolution of mercury droplets in aqueous media seem to be complex, and a complete understanding of this process needs the study of (i) formation of oxygen–mercury activated complexes at the surface of the droplets, (ii) electron transfer reactions, (iii) formation of a mercury oxide film, and (iv) dissolution of this film with consequent release of Hg(II) to the solution. This requires evaluation of the kinetics of surface oxidation reactions, the identification of surface species, and study of the dissolution behavior of oxygen–mercury compounds in aqueous media.

The aim of this article is to study the dissolution behavior of montroydite (the most representative form of HgO in nature) in order to gain a better understanding of both its behavior in contaminated sites, where it occurs at important concentrations, and the dissolution behavior of possible oxygen–mercury species that may form at the liquid Hg^0/solution interface. The thermodynamics and mainly the kinetics of HgO dissolution in an inert electrolyte medium are investigated. The data obtained at a variety of pH, stirring rate, and temperature conditions are used to elucidate the respective effects of transport and reaction control on the overall dissolution rate. Besides giving information about the behavior of mercury in the environment, the study also helps in understanding the basic principles of metal oxide dissolution by drawing a quantitative link between the mechanisms of metal removal from a dissolving mineral surface and the mechanism of water exchange from the hydration sphere of the corresponding hydrated metal ion in solution.

2. Materials and methods

2.1. Materials

Red and yellow HgO (purity $\geqslant 99\%$) were purchased as powder reagents from Fluka (Product Numbers 83373 and 83382, respectively) and used without further treatment. X-ray diffraction analysis and Rietveld refinement indicated that they are mineralogically pure and have the hexagonal orthorhombic crystal structure corresponding to the montroydite mineral. Scanning electron microscope images, obtained with a JEOL 35CF microscope equipped with a secondary electron detector, showed that red HgO consists of well crystalline prismatic particles with a size of around 2 μm, which appear to be fused together, forming rounded multiparticle aggregates around 20 μm in diameter. Yellow HgO consists of somewhat smaller particles of around 1 μm, having a less defined shape and forming smaller aggregates of about 5 μm. The specific surface areas were 0.45 and 0.68 m^2/g for the red and yellow HgO as measured by N_2 adsorption (BET method).

All solutions were prepared with 18-MΩ ultrapure water (Milli-Rho Milli-Q system), which was boiled and degassed before the experiments to prevent CO_2 contamination. Analytical grade reagents were used in all cases: KOH, HNO_3, and KNO_3 (Merck), dithizone (Riedel-de-Haën), and triton X-100 (Anedra). pH 4.00, 7.00, and 10.00 buffers (Anedra) were used to calibrate the glass electrode.

2.2. Analytics

Total Hg(II) concentration was measured spectrophotometrically by the fully automated method developed by Garrido et al. [9]. Briefly, the aqueous Hg(II) solution was withdrawn from the dissolution vessel (or from the centrifuge tube) at a flow rate of 0.25 $ml\,min^{-1}$ with PVC tubing connected to a peristaltic pump (Gilson Miniplus 3) and mixed with a dithizone solution in Triton X-100 at pH 2. The dithizone solution was generated on line by flowing a 5% v/v Triton X-100 solution through a column containing solid dithizone. Under these conditions, the complexation of Hg(II) with dithizone produces a colored species that can be detected spectrophotometrically at a wavelength of 500 nm [9]. The tubing used to withdraw the Hg(II) solution was capped with glass wool to ensure that all HgO particles remained in the dissolution vessel. Once formed, the solution containing the colored Hg(II)–dithizone complex was flown to a Hellma 178712-QS quartz cell and detected with a Hewlett Packard 8452A diode array spectrophotometer. The spectrum of the solution was recorded every 2 s in the wavelength range 300–800 nm, and the concentration of Hg(II) was determined from the absorbance at 500 nm. The detection limit of the method is around 10^{-7} M.

2.3. Dissolution experiments

Two kinds of dissolution experiments were performed: solubility experiments, to measure the thermodynamic solubility of HgO as a function of pH, and dissolution kinetics experiments, to measure the dissolution rate of HgO as a function of pH, temperature, and stirring rate.

Both red and yellow HgO were used in solubility experiments. Portions of 0.5 g of solid were placed in 50-ml centrifuge tubes and 40 ml of a 0.010 M KNO_3 solution were added to each tube. The pH of the dispersions was adjusted to the desired value by adding either HNO_3 or KOH solutions, and the tubes were then continuously shaken until equilibrium was reached. Although preliminary experiments showed that a few minutes was enough to reach equilibrium, suspensions were shaken for at least 3 h. After this time, the suspension was centrifuged and

the supernatant withdrawn for total mercury analysis and pH measurement. The pH range investigated was 2.2–10.1. All solubility experiments were performed at 23 °C (with a standard deviation of 1 °C). The temperature was controlled with a Julabo thermostatic bath. Although solubility can be approached both from undersaturation and from supersaturation, studies from supersaturation were not performed here, to avoid any possible precipitation of a solid phase different from montroydite, which would complicate the analysis of data.

Red HgO was used for dissolution kinetics experiments. They were begun by adding 20 mg of solid to a thermostated glass reaction vessel containing 100 ml of a 0.010 M KNO_3 solution, whose pH was set to the desired value by adding HNO_3 or KOH solution. The temperature was maintained constant with a bath that circulated water through an exterior jacket surrounding the reaction vessel. The dispersion was stirred with a magnetic bar at 220 rpm, and the pH was continuously measured and corrected if changes were observed. However, since the amount of solid used was relatively low, pH changes due to proton consumption by dissolution were always smaller than 0.1 pH unit. Minute portions of the reactor solution were extracted during the experiments by the peristaltic pump and used for total Hg(II) quantification as described above. Most of the dissolution kinetics experiments were performed at 23 °C. The effect of pH in the range 2.4–10.1 and of stirring rate in the range 35–450 rpm were investigated at this temperature. In addition, the effects of temperature in the range 4–49 °C at pH 3.5 and stirring rate 220 rpm were also investigated.

Additional dissolution kinetics experiments at pH 2.7 were performed as described above, but placing only 10 mg of solid in the reaction vessel. This low amount of solid was chosen to ensure that the whole dissolution run took place away from the solubility limit of HgO (the complete dissolution of 10 mg of HgO in 100 ml solution leads to a total Hg(II) concentration of 4.6×10^{-4} M, whereas the solubility of HgO at pH 2.7 is 2×10^{-3} M). Since almost complete dissolution of the studied solid can be achieved under these conditions, the shape of the dissolution curves can be evaluated (see below).

In all the experiments, pH values were measured with an ORION 710A pH meter equipped with an ORION 81-02 Ross electrode. Buffer solutions were equilibrated at the working temperature before electrode calibration.

2.4. The model

Dissolution of minerals such as montroydite may occur in different steps [10–13]: (1) mass transfer of dissolved reactants (e.g., protons) from the bulk solution to the mineral surface, (2) adsorption of these reactants to the mineral surface, (3) interlattice transfer of reacting species and formation of the activated complex, (4) surface chemical reactions, and (5) mass transfer of the reaction products into the bulk solution. Any one or more of these steps can be rate-controlling, but it is customary to identify the kinetic processes as either transport-controlled processes (where step (1) or (5) is the rate-limiting step) or surface-controlled processes (where step (2), (3), or (4) is the rate-limiting step).

Transport steps and surface steps proceed simultaneously when dissolution is taking place. This means that after a very small time a steady state occurs and the rate of transport steps equals the rate of surface steps, regardless of the controlling process [12]. This equality of the various rates is required to ensure that no dissolution product accumulates at the mineral/water interface.

The transport to and from the surface depends on the hydrodynamics of the system under investigation. In the case of a well-stirred solution near the mineral surface, the transport is determined by a stagnant layer through which diffusion takes place according to the second Fick law. The diffusion of material is caused by the concentration gradient between the bulk and the surface. This can be written as [14]

$$J = k_t(c_s - c_b), \tag{1}$$

where J is the material flux, k_t is a transport rate coefficient, c_b is the concentration of dissolved material in the bulk solution, and c_s is its concentration at the surface. The value of k_t mainly depends on the thickness of the stagnant layer and on the diffusion coefficient of the reacting species. The thickness of the stagnant layer can be changed, for instance, by changing the stirring rate. The diffusion coefficient may also change when the reacting species change. For example, if the dissolving conditions (such as pH) are modified, the species that are being transferred from the surface to the bulk solution will also change (for example, Hg^{2+} at low pH and $Hg(OH)_2^0$ at high pH). k_t will thus change if these species have different diffusion coefficients. However, this does not appear to be the case for dissolving metal oxides, since either nonhydroxylated or hydroxylated dissolved metal ions have similar diffusion coefficients [10], and thus k_t can be considered independent of pH.

Following Lasaga [10], the surface reaction rate can be expressed as

$$R_s = k_s(c_{eq} - c_s)^n, \tag{2}$$

where R_s is the surface reaction rate, k_s is a surface rate coefficient, c_{eq} is the equilibrium bulk concentration of the soluble species (soluble Hg(II) species in our case), and n is a real number. In the analysis of our experimental data we found that $n = 1$; thus we remove it from the equations to simplify their solution. From Eq. (1) the following expression for c_s can be obtained:

$$c_s = \frac{J}{k_t} + c_b. \tag{3}$$

Substituting in Eq. (2) and rearranging,

$$R_s + \frac{k_s J}{k_t} = k_s c_{eq} - k_s c_b. \tag{4}$$

Knowing that R_s must equal J, Eq. (4) can be rearranged to give

$$R = \frac{k_s k_t}{k_s + k_t}(c_{eq} - c_b), \tag{5}$$

where R is the overall reaction rate ($R = J$ in a transport-controlled process and $R = R_s$ in a surface-controlled process).

Equation (5) indicates that dissolution takes place when $c_b < c_{eq}$ and that formation of solid takes place when $c_b > c_{eq}$.

Additionally, since $c_b = 0$ at the beginning of a dissolution experiment, the initial dissolution rate, R_0, is given by

$$R_0 = \frac{k_s k_t}{k_s + k_t} c_{eq}, \tag{6}$$

which indicates that the initial dissolution rate is proportional to c_{eq}. Then an R_0 vs pH curve should have the same shape as the solubility curve (c_{eq} vs pH).

On the other hand, when $k_t \ll k_s$, the initial dissolution rate is given by

$$R_0 = k_t c_{eq}, \tag{7}$$

which indicates that the process is transport-controlled. On the contrary, when $k_t \gg k_s$, the equation for a surface-controlled process is obtained:

$$R_0 = k_s c_{eq}. \tag{8}$$

Between these two limiting cases, Eq. (6) must be applied.

Dissolution kinetics experiments performed in this work made it possible to monitor the increase in the total supernatant concentration of Hg(II) species as a function of time. This total concentration of species can be identified as c_b, according to the nomenclature used above. Thus, R can be evaluated at any time from the slope of a c_b vs t curve:

$$R = \frac{dc_b}{dt}. \tag{9}$$

In addition, the degree of progress of the dissolution reaction, α, can also be evaluated, and can be defined as

$$\alpha = \frac{W_0 - W}{W_0} = \frac{V_0 - V}{V_0}, \tag{10}$$

where W and V are respectively the mass and volume of solid remaining undissolved at a certain time t, and W_0 and V_0 are respectively the initial mass and volume of solid used in the dissolution run. The value $\alpha = 0$ means that 0% of the solid has been dissolved, whereas $\alpha = 1$ means that 100% of the solid has been dissolved.

3. Results and discussion

3.1. Solubility of HgO

Fig. 1 shows the solubility of both red and yellow mercury oxides as a function of pH in 0.01 M KNO_3 solutions. Although a small difference in solubility between the oxides is reported in the literature [15], no significant differences were found in the present study. We shall therefore discuss hereafter the dissolution thermodynamics and kinetics of red HgO only. The data are in good agreement with previous results compiled by Baes and Mesmer [15]. Experimental data in Fig. 1 are compared with a solubility curve computed with the MINEQL$^+$ code [16], using the Davies equation for the activity coefficients and equilibrium constants reported by Baes and Mesmer [15]. The solubility is constant and equal to 2.05×10^{-4} M above pH 4, and increases sharply as pH decreases below pH 4, reaching a value

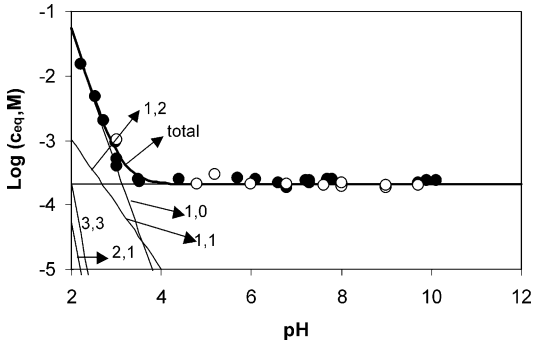

Fig. 1. Solubility curve for HgO at 23 °C in 0.01 M KNO_3 solutions. Experimental data for red HgO (filled circles) and yellow HgO (empty circles) are compared to the solubility curve (thick line) computed with the MineQL$^+$ code. Contribution by individual $Hg_x(OH)_y$ species to the total solubility are shown by individual line (thin lines) identified by the x, y stoichiometric coefficients.

of 5.49×10^{-2} M at pH 2. The distribution of soluble species contributing to the total mercury solubility is also shown in Fig. 1. Two species dominate this speciation: Hg^{2+} dominates at pH < 2.6, and $Hg(OH)_2^0$ dominates at pH > 3.6, whereas both species are significant in the pH range 2.6–3.6.

The solubility of montroydite is relatively high compared to that of many other metal oxides present in nature. For instance, the solubility minima for Al(III), Fe(III), Fe(II), and Mn(II) oxides are about 10^{-6}, 10^{-11}, 10^{-6}, and 10^{-5} M, respectively [15], while the solubility minimum of HgO (observed at pH > 4) is equal to 2.05×10^{-4} M. This solubility is much higher than that of cinnabar (HgS, solubility about 10^{-19} M), and accounts in part for the fact that Hg(II) is commonly present in solid phases mainly as sulfide or selenide compounds, which are highly insoluble, and less as HgO, which is found only in highly contaminated sites such as gold mines [3].

The magnitude of the solubility of HgO also gives some clues about the mode (transport or surface reaction) that controls the dissolution rate of the solid. Indeed, and following Lasaga [12], a theoretical rule of thumb proposed by Berner [17] states that for aqueous solutions, minerals with low solubility dissolve by surface control, whereas highly soluble minerals dissolve by transport control. Examples of minerals with low solubility and surface control are $BaSO_4$ (solubility 1×10^{-5} M) [12], aluminum oxide [13], iron(III) oxide [13], and others [12]. Examples of minerals with high solubility and transport control are $CaSO_4 \cdot 2H_2O$ (solubility 5×10^{-3} M), $Na_2SO_4 \cdot 10H_2O$ (solubility 0.2 M), and others [12]. Minerals that have intermediate solubility, such as $PbSO_4$ (solubility 1×10^{-4} M), seem to have mixed control (transport and surface) of the dissolution reaction [12]. Thus, mixed control can be envisaged for HgO from solubility data, although this conclusion needs to be confirmed from kinetic data.

3.2. Measuring dissolution kinetics of HgO

Fig. 2 shows the changes in the UV–vis spectra of the supernatant solution (after reacting with dithizone) during a typical dissolution kinetics experiment. This kind of plot was used to monitor the increase in the concentration of dissolved mercury

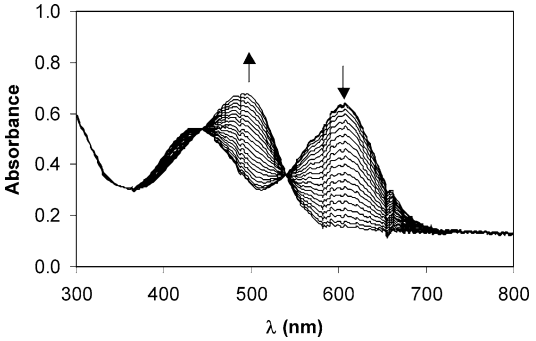

Fig. 2. Supernatant UV–vis spectra recorded at different times during the dissolution of red HgO at 23 °C in a pH 3.5, 0.01 M KNO_3 ionic medium. The arrows indicate the direction of changing spectra with time.

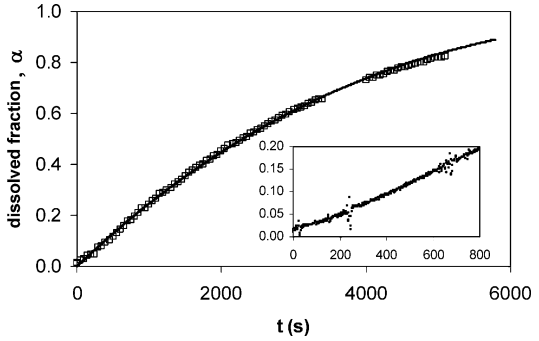

Fig. 3. Dissolution curve of red HgO. Initial solid concentration 10 mg/100 ml, pH 2.7, temperature 23 °C, stirring rate 220 rpm. Experimental data (symbols) are compared to predictions of Eq. (11) (line) with $k/r_0 = 9 \times 10^{-5}$ cm^{-1}. One out of 50 experimental points was omitted for clarity. The inset of the figure shows all the experimental data between $t = 0$ s and $t = 800$ s.

as a function of time. At short reaction times the spectral curves correspond to the spectrum of pure dithizone (which has a maximum at 608 nm), indicating that the concentration of mercury species in the supernatant is negligible. As the dissolution proceeds, there is a decrease in the absorbance at 608 nm together with an increase in the absorbance at 500 nm. The maximum at 500 nm corresponds to the maximum of the dithizone–Hg(II) complex, indicating that mercury species appear in the supernatant as time increases.

The isosbestic points at 445 and 540 nm suggest that only two species absorb light in the studied wavelength range [18], namely, dithizone and the dithizone–Hg(II) complex. Therefore, analysis of the spectral changes made it possible to quantify total mercury concentration in the supernatant and to construct dissolution curves by plotting either c_b vs t or α vs t.

3.3. The shape of the dissolution curve

In dissolution kinetics studies, it is a common practice to analyze the behavior of a solid by measuring its initial dissolution rate, which is obtained from data recorded at the beginning of the dissolution run. However, in many cases this initial dissolution rate may not reflect the actual dissolution behavior of the studied material, since at the very beginning of the process the rate may be affected by factors whose origin and consequences are seldom well understood and controlled, such as the presence of some surface impurities, minute amounts of fast-dissolving amorphous particles, surface defects, or transient periods before steady state is reached. It is always convenient to check the behavior of the sample from the very beginning to nearly the end of the dissolution process [19]. This makes it possible to obtain a complete dissolution curve, whose shape can be analyzed in order to detect the presence of undesired processes and induction times that can affect data interpretation.

Fig. 3 shows the dissolution curve of 10 mg of HgO at pH 2.7. Dissolution was followed from the very beginning ($\alpha = 0$) to nearly the end of the process ($\alpha = 0.85$). At the beginning ($0 < \alpha < 0.05$), an induction time with a relatively low dissolution rate was found. This interval can be well observed in the inset of the figure. Factors responsible for this induction time are not well understood. Perhaps some surface hydration is affecting the results in this period, but there is no clear evidence for this or other processes. Thus, induction times are not considered in evaluating the dissolution rate of HgO. After this induction time, the slope of the α vs t curve acquires its maximum value, which then decreases monotonically as t increases. Neglecting the data belonging to the induction time, the curve takes the shape of the equation

$$1 - (1 - \alpha)^{1/3} = \frac{k}{r_0} t, \tag{11}$$

which represents the dissolution of a spherical particle, where r_0 is its initial radius and k is a constant. Equation (11) is derived in Appendix A for spherical particles, although it can also be derived for any other isometric three-dimensional body [19]. For example, the same equation can be obtained for cubic particles with the corresponding substitution of r_0 by the initial cube length. Derivation of Eq. (11) assumes that the dissolution rate of the particle is proportional to its surface area. Therefore, as dissolution proceeds, the particle and its surface area become smaller, and this is why the dissolution rate decreases monotonously with time. This dissolution mechanism is known as the three-dimensional contracting mechanism or attrition mechanism [20] and implies that the hypothetical spherical particle is keeping its shape during dissolution, k representing the constant rate at which its radius is decreasing. For the example shown in Fig. 3, assuming that the dissolving entities are individual HgO crystals with $r_0 = 2$ μm, the radius of the crystals should decrease at a constant penetration rate $k = 0.000180$ μm s^{-1} or 0.648 μm h^{-1}. On the other hand, assuming that the dissolving entities are the aggregates ($r_0 = 10$ μm) seen by electron microscopy, their radii should decrease at a constant penetration rate $k = 0.00090$ μm s^{-1} or 3.24 μm h^{-1}. Actually, the Fig. 3 data do not make it possible to prove whether the dissolving entities are single crystals or whole aggregates. However, preliminary granulometric studies indicate that the aggregates are still present during dissolution, suggesting that they are the dissolving entities. Since montroydite crystals are fused together in random orientations in the original aggregates, the penetration rate estimated with the value of k is actually an averaged penetration rate of the outer surface of the aggregates.

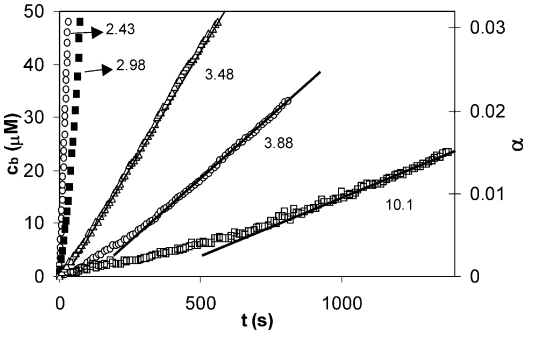

Fig. 4. Dissolution curve of red HgO obtained at different pH values. Temperature 23 °C, stirring rate 220 rpm. Initial solid concentration 20 mg/100 ml. pH values are given in the figure.

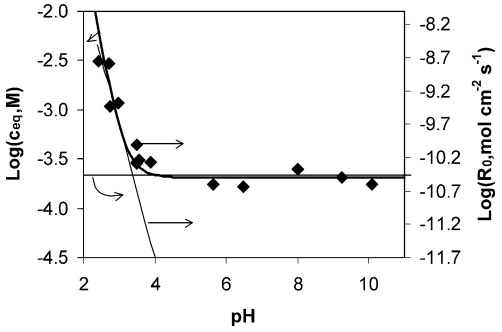

Fig. 5. Initial dissolution rates (symbols) and solubility (thick line) of HgO as a function of pH. Thin lines represent the two components of the empirical rate law, as described by Eq. (14), with $R_W = 3.5 \times 10^{-11}$ mol cm^{-2} s^{-1} (flat line), $k_H = 2.0 \times 10^{-4}$ L^2 mol^{-1} cm^{-1} s^{-1}, and $n = 2$ (negative slope line).

3.4. Effect of pH, stirring rate, and temperature

Fig. 4 shows dissolution kinetics experiments performed at different pHs. Induction times are observed in all curves. In order to compare dissolution rate data, the initial rate was assumed to be the slope of the c_b vs t curves after the induction time, which is the slope of the straight lines drawn in the figure.

At pH 10.1 and down to pH 4 (data not shown), the rate does not depend on pH, whereas at pH values below pH 4 the rate increases significantly as pH decreases. Fig. 5 reports the initial dissolution rates (obtained from data such as those in Fig. 4) as a function of pH and compares them to the thermodynamic solubility curve. The shape of both curves is similar, in agreement with the predictions of Eq. (11). The proportionality factor, i.e., the value of the $k_s k_t/(k_s + k_t)$ parameter, is 2.0×10^{-4} cm s^{-1}.

Since $k_s k_t/(k_s + k_t)$ is composed of k_s and k_t, it is desirable to evaluate the k_s and k_t contributions to this parameter. This is important because k_s is a value that depends only on the HgO properties, and thus it can be used and applied in any situation where HgO dissolution in aqueous media is evaluated. Once k_s is known from laboratory data, this value can be applied to natural systems and field data, combined with the corresponding transport constant [10]. The value of k_s was estimated by investigating the effect of the stirring rate on the dissolution rate. The results obtained at pH 3.5 are plotted in Fig. 6. They show an increase of the initial dissolution rate with increasing stirring rate. In addition, stabilization of the overall rate is envisaged at

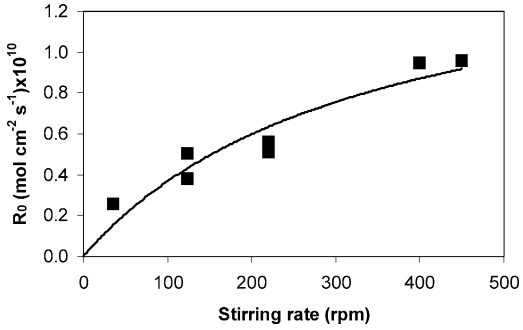

Fig. 6. Initial dissolution rate of red HgO as a function of the stirring rate. Experimental data (symbols) and theoretical data (line) calculated with Eq. (12) with $A = 1.51 \times 10^{-6}$ cm s^{-1} rpm^{-1} and $k_s = 5.05 \times 10^{-4}$ cm s^{-1}. pH 3.5, temperature 23 °C.

high stirring rates. Assuming k_t proportional to the stirring rate, Eq. (6) can be rewritten as

$$R_0 = \frac{k_s A S}{k_s + A S} C_{eq}, \tag{12}$$

where S is the stirring rate and A is the proportionality constant between k_t and S. Equation (12) can be linearized to give

$$\frac{C_{eq}}{R_0} = \frac{1}{AS} + \frac{1}{k_s}; \tag{13}$$

thus A and k_s can be estimated respectively from the slope and the y-intercept of a C_{eq}/R_0 vs $1/S$ plot (not shown). The line in Fig. 6 is a plot of Eq. (12) with the estimated values $A = 1.51 \times 10^{-6}$ cm s^{-1} rpm^{-1} and $k_s = 5.05 \times 10^{-4}$ cm s^{-1}. An acceptable fit ($R^2 = 0.85$) was obtained. This fit is better than the one that could be obtained by fitting data in Fig. 6 with a straight line ($R^2 = 0.77$), indicating that the curve tends to level off at high stirring rates. The fact that the value of k_s is similar to the values of k_t, which varies from 5.28×10^{-5} to 6.79×10^{-4} cm s^{-1} in the whole range of stirring rates investigated, indicates that the dissolution kinetics is controlled by a combination of transport and surface reactions, in agreement with the conclusions obtained from solubility data. Only at much higher stirring rates, which could not be reached with the experimental setup used in this work, would the dissolution rate represent a pure surface-controlled process, with $R_0 = k_s c_{eq} = 1.6 \times 10^{-10}$ mol cm^{-2} s^{-1} (see Eq. (8)) at pH 3.5.

The dissolution rate of red HgO at pH 3.5 and stirring rate 220 rpm increases by more than one order of magnitude as the temperature increases from 5 to 49 °C. An Arrhenius plot was constructed to estimate the apparent activation energy of the process, E_a, by plotting the logarithm of $k_s k_t/(k_s + k_t)$ (or R_0/c_{eq}) as a function of $1/T$, where T is the absolute temperature. Values for c_{eq} at different temperatures were calculated with the MINEQL$^+$ code [16]. This plot is shown in Fig. 7, whose slope makes it possible to calculate an apparent activation energy $E_a = 35.9$ kJ/mol. According to Lasaga [10, 12], diffusion-controlled reactions in aqueous media have rather low activation energies ($E_a < 20$ kJ/mol), whereas activation energies that are much higher are indicative of a chemical surface-controlled process. For instance, gibbsite dissolution in acidic medium was characterized by an E_a value ranging from

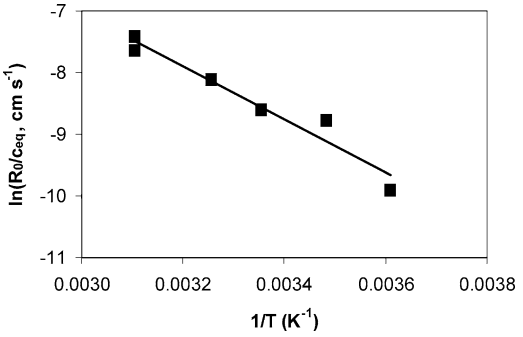

Fig. 7. Arrhenius plot for the dissolution of red HgO. pH 3.5, stirring rate 220 rpm.

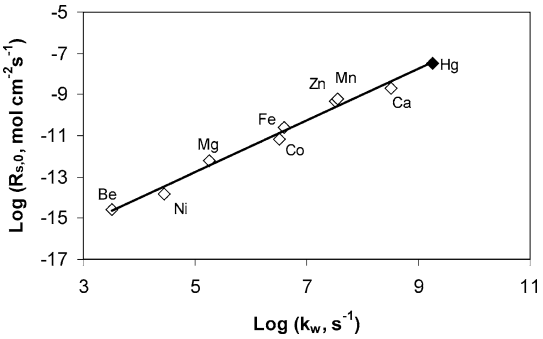

Fig. 8. Comparison of the proton-promoted dissolution rate of divalent metal oxides with the first-order rate coefficient for water exchange (k_w) of the corresponding cations in aqueous solutions. $R_{s,0}$ represents the initial surface-controlled dissolution rate. Data obtained from Casey [25] are represented with empty symbols. Data for red HgO are those obtained in this article.

59 ± 4.3 to 67 ± 0.6 kJ/mol and is clearly a surface-controlled reaction [21]. The value of $E_a = 35.9$ kJ/mol, which is intermediate between normal activation energies for transport-controlled and surface-controlled processes, also indicates that under the conditions studied in this work, HgO dissolution is not a purely surface-controlled process and that both surface reactions and transport control the dissolution kinetics. This mixed control seems to be usual for many minerals. Indeed, the same characteristics (high solubility, fast dissolution, and mixed controlled kinetics) were observed for calcite [$CaCO_3$(s)] [22,23]. The only way found to characterize the surface-controlled reaction rate for this mineral was to stick a crystal on a rotating disk and to study the dissolution under conditions where transport no longer controls the dissolution phenomenon [22,23].

3.5. Dissolution mechanism

The dissolution mechanisms of most of the oxide minerals are viewed as progressive ligand-exchange reactions. The bridging oxygens that link the cation to the mineral surface are progressively replaced by functional groups until a small aqueous complex detaches [13,24,25]. In the case of proton-promoted dissolution in oxide minerals, there are several fast surface protonation steps at oxygens surrounding the metal center, followed by slow hydration and detachment steps, one of these hydration steps being the rate-controlling one. These protonation and ligand-exchange reactions lead to the formation of monomeric species at the surface (e.g., $Ni(OH_2)_6^{2+}$ or $Al(OH_2)_6^{3+}$ for the respective dissolution of NiO or Al_2O_3) that move from the surface to the bulk solution [24]. The mechanism suggests that the local bonding environment of the metal ion and oxygen is an important factor controlling the dissolution rate. Thus, the variables that influence the rate of ligand exchange may also be important in controlling the dissolution rate [26].

The best evidence for this mechanism comes from the observation that the rates of oxide dissolution scale like the rate of water exchange around the corresponding cation in solution [24,25]. This relationship can be seen in Fig. 8, where the proton-promoted dissolution rate of oxides is plotted as a function of the first order rate coefficient for water exchange of different divalent cations. The data for all cations except mercury were taken from Casey [25] and correspond to surface-controlled dissolution rates at pH close to 1 or 2 [26]. The solid symbol corresponds to the dissolution rate of HgO, which was obtained by extrapolating to pH 2 the surface-controlled rate $R_0 = k_s c_{eq} = 1.6 \times 10^{-10}$ mol cm^{-2} s^{-1} obtained at pH 3.5. The rate coefficient for water exchange (1.8×10^9 s^{-1}) was taken from Inada et al. [27]. Mercury data fit the trend shown by the other cations well, suggesting that the dissolution mechanism of HgO is also a ligand-exchange mechanism where hydration steps are rate-controlling.

3.6. Empirical rate laws

The rates of oxides dissolution are usually described in terms of empirical rate laws that include rate coefficients, the concentration of either reactants in solution (such as protons) or adsorbed reactants (such as adsorbed protons), and reaction orders. For example, in the particular case of the dissolution kinetics of simple oxide minerals, such as NiO, BeO, and Al_2O_3, the surface-controlled kinetics is governed by the equation [13, 25,28]

$$R = R_w + k_H[H^+]^n + \cdots, \tag{14}$$

where the total dissolution rate, R, is given by the sum of several terms, each one representing the contribution of different processes acting in parallel, such as proton-promoted dissolution, ligand-promoted dissolution, etc. In Eq. (14), for example, the first term of the right-hand side corresponds to a pH-independent rate given by R_w, and the second term is the proton-promoted dissolution, k_H and n being respectively a dissolution rate coefficient and the order of the reaction with respect to aqueous proton concentration, $[H^+]$. In the case of proton-promoted dissolution n takes typically values between 0 and 0.5 [29]. R_0 vs pH data shown in Fig. 5 can be described well with the first two terms of Eq. (14), with the following values: $R_w = 3.5 \times 10^{-11}$ mol cm^{-2} s^{-1}, $k_H = 2.0 \times 10^{-4}$ L^2 mol^{-1} cm^{-1} s^{-1}, and $n = 2$. The predictions are shown in the same figure.

These rate laws seem to be quite general not only for oxides but also for other minerals. Indeed, Plummer et al. [30]

and Van Cappellen et al. [31] used the same kind of equation for calcite dissolution at constant CO_2 pressure. This was interpreted as evidence for several distinct dissolution reactions, such as a proton-promoted reaction and a (H_2O+CO_2)-induced dissolution reaction leading to the release of Ca^{2+} and HCO_3^-. In the same manner, the rate law for red HgO indicates that dissolution of the oxide may occur by two processes operating in parallel, with the overall rate reflecting the contribution from the following two processes:

$$HgO(s) + 2H^+(aq) = Hg^{2+}(aq) + H_2O(l), \quad (15)$$

$$HgO(s) + H_2O(l) = Hg(OH)_2^0(aq). \quad (16)$$

While reaction (15) occurs whatever the pH is, reaction (16) starts to be significant and dominant only at low pH.

If instead of expressing the rate as a function of proton concentration in solution, it is expressed as a function of adsorbed proton ions (c_s^H), the rate law takes the form

$$R = R_w + k_H\left(c_s^H\right)^n + \cdots, \quad (17)$$

and n takes integer values, which commonly equal the valence state of the metal in the oxide (e.g., $n = 2$ for the proton-promoted dissolution of NiO and BeO, and $n = 3$ for that of Al_2O_3). This interesting behavior allowed Furrer and Stumm [28] to conclude that two (for the case of divalent metal oxides) or three (for the case of trivalent metal oxides) fast protonation steps take place before the rate-controlling hydration and detachment steps. This behavior is observed at pH $\ll$ PZC (point of zero charge of the oxides), where the term corresponding to the proton-dissolution rate is dominant. Under these conditions, the detaching surface complex resembles the fully hydrated metal ion [24]. Closer to the PZC, however, hydrolyzed metal ion dissolution products must be taken into account and n may differ significantly from the valence of the free metal ion. It could tend toward zero or even become negative at pH values larger than PZC, where negatively charged hydrolyzed species are formed [24]. For example, if in the case of NiO the detaching species are either $Ni(OH_2)_6^{2+}(aq)$, $Ni(OH)(OH_2)_5^+(aq)$, or $Ni(OH)_2(OH_2)_4^0(aq)$, the respective rate orders in Eq. (17) will be 2, 1, or 0.

To write a rate law where the dissolution rate is expressed as a function of proton concentration at the oxide surface it is necessary to perform proton adsorption measurements at different pHs, aiming to determine c_s^H at those pHs. This can be done with acid–base potentiometric titration when the solubility of the studied solid is low. We tried to perform this kind of titration with our HgO sample. However, the results were unfruitful because of the high and fast dissolution of the oxide. The only proton consumption that we detected in our titration experiments was due to oxide dissolution, and this impeded obtaining reliable proton adsorption data. Even though it is not possible to write an empirical rate law such as Eq. (17), dissolution data of HgO indicates that the mercury species that are being transferred from the surface to the bulk solution correspond to the species that are more stable and dominant at the studied pH (i.e., the transferred species at very low pH is mainly aqueous Hg^{2+}, whereas the one transferred at pH > 4 is mainly aqueous $Hg(OH)_2^0$). The similarity in the shapes of the rate vs pH and the solubility vs pH curves supports this reasoning.

4. Conclusions

The following conclusions can be drawn from the present study:

The fully automated method developed by Garrido et al. [9], which combines batch reaction with dithizone complexation of soluble Hg(II) species, can easily be adapted to monitor HgO dissolution kinetics in an ample range of pH, stirring rate, and temperature.

The dissolution rate of montroydite does not depends on pH between 4 and 10 but increases markedly at pH < 4. The dissolution process obeys the three-dimensional contracting mechanism.

Both solubility data and dissolution kinetic data indicate that under the experimental conditions used in this work, the dissolution is controlled by a combination of surface and transport processes, such as occurs with other highly soluble minerals as calcite. In spite of this, the respective effects of the transport and reaction control on the overall dissolution rate could be evaluated.

Comparison with the behavior of other divalent metal oxides indicates that the dissolution rate of HgO at low pH is relatively high. At pH 2 the dissolution rate of these oxides scales with the rate of water exchange, suggesting that the steps that control the detachment of Hg(II) species from the montroydite mineral surface are ligand exchange reactions. The high dissolution rate is a consequence of the ability of Hg(II) to rapidly exchange its ligands.

The use of a simple model combining transport and surface reactions (Eq. (6)), or the use of empirical rate laws, makes it possible to conclude that mercury species that are being transferred from the surface to the bulk solution correspond to the species that are more stable and dominant at the studied pH. Thus the transferred species at very low pH is mainly aqueous Hg^{2+}, whereas the one transferred at pH > 4 is mainly aqueous $Hg(OH)_2^0$.

The relatively high thermodynamic solubility of montroydite, together with its relatively high dissolution rate, explains why HgO is not commonly found in the environment. It only occurs in highly contaminated sites. These properties of HgO also suggest that oxygen–mercury species that form at the surface of liquid Hg droplets can dissolve rapidly in aqueous media.

Acknowledgments

A.H. acknowledges a Ph.D. study fellowship given both by the Region Rhône-Alpes (France) and by the University of Cordoba (Argentina). Partial financial support was provided to L.C. and M.A. by a MIRA project (Région Rhône-Alpes) and Ecos-Secyt, and to L.C. by the "Mercury in French Guyana—Part II" project (Région Guyane and MEDD). M.A. also thanks CONICET and FUNDACIÓN ANTORCHAS.

Appendix A

The dissolution rate of a spherical homogeneous particle is assumed to be proportional to its surface area (S). Thus,

$$\frac{dV}{dT} = -kS, \tag{A.1}$$

where V is the volume of the particle and t is time. In addition, the surface of a sphere is related to its volume through

$$S = 4\pi\left(\frac{3}{4\pi}\right)^{2/3} V^{2/3}. \tag{A.2}$$

Substituting this equality into (A.1) and rearranging,

$$\frac{dV}{V^{2/3}} = -k4\pi\left(\frac{3}{4\pi}\right)^{2/3} dt. \tag{A.3}$$

Upon integration,

$$V^{1/3} - V_0^{1/3} = -k\left(\frac{4\pi}{3}\right)^{1/3} t, \tag{A.4}$$

where V_0 is the volume of the particle at $t = 0$. Dividing (A.4) by $V_0^{1/3}$,

$$\frac{V^{1/3} - V_0^{1/3}}{V_0^{1/3}} = -k\left(\frac{4\pi}{3V_0}\right)^{1/3} t. \tag{A.5}$$

Expressing the right-hand side of Eq. (A.5) in terms of the initial radius of the particle, r_0, the following equation results:

$$\frac{V^{1/3} - V_0^{1/3}}{V_0^{1/3}} = -\frac{k}{r_0} t. \tag{A.6}$$

From the definition of α according to Eq. (10), the left-hand side of (A.6) can be changed to give

$$(1-\alpha)^{1/3} - 1 = -\frac{k}{r_0} t, \tag{A.7}$$

from which the desired Eq. (11) is obtained.

References

[1] M.E.A. de Magalhães, M. Tubino, Sci. Total Environ. 170 (1995) 229.
[2] T. Peretyazhko, L. Charlet, B. Muresan, V. Kazimirov, D. Cossa, Sci. Total Environ., in press.
[3] C.S. Kim, N.S. Bloom, J.J. Rytuba, G.E. Brown, Environ. Sci. Technol. 37 (2003) 5102.
[4] R.N. Sliger, J.C. Kramlich, N.M. Marinov, Fuel Process. Technol. 65–66 (2000) 423.
[5] G.A. Norton, H. Yang, R.C. Brown, D.L. Laudal, G.E. Dunham, J. Erjavec, Fuel 82 (2003) 107.
[6] M. Amyot, F.M.M. Morel, P.A. Ariya, Environ. Sci. Technol. 39 (2005) 110.
[7] Z. Wang, S.O. Pehkonen, Atmos. Environ. 38 (2004) 3675.
[8] M. Yamamoto, Chemosphere 31 (1995) 2791.
[9] M. Garrido, M.S. Di Nezio, A.G. Lista, M. Palomeque, B.S. Fernández Band, Anal. Chim. Acta 502 (2004) 173.
[10] A.C. Lasaga, Kinetic Theory in the Earth Sciences, Princeton Univ. Press, Princeton, NJ, 1997.
[11] D.L. Sparks, Kinetics of Soil Chemical Processes, Academic Press, San Diego, 1988.
[12] A.C. Lasaga, in: M.F. Hochella Jr., A.F. White (Eds.), Mineral–Water Interface Geochemistry, in: Reviews in Mineralogy, Mineralogical Soc. Am., Washington, 1990 (ch. 2).
[13] W. Stumm, Processes at the Mineral–Water and Particle–Water Interface in Natural Systems, Wiley–Interscience, New York, 1992 (ch. 5).
[14] M.A. Cohen Stuart, A. de Keizer, in: J. Wingrave (Ed.), Oxide Surfaces, in: Surfactant Science Series, vol. 103, Dekker, New York, 2001, pp. 157–199.
[15] C.F. Baes, R.E. Mesmer, The Hydrolysis of Cations, Wiley–Interscience, New York, 1976.
[16] W.D. Schecher, D.C. McAvoy, MINEQL$^+$: A Chemical Equilibrium Program for Personal Computers, User's Manual, Version 3.0, Environmental Research Software, Hallowell, 1994.
[17] R.A. Berner, Am. J. Sci. 278 (1978) 1235.
[18] K.A. Connors, Binding Constants. The Measurements of Molecular Complex Stability, Wiley–Interscience, New York, 1987.
[19] M.A. Blesa, P.J. Morando, A.E. Regazzoni, Chemical Dissolution of Metal Oxides, CRC Press, Boca Raton, FL, 1993.
[20] M.J. Avena, K.J. Wilkinson, Environ. Sci. Technol. 36 (2002) 5100.
[21] P.R. Bloom, M.S. Erich, Soil Sci. Soc. Am. J. 51 (1987) 1131.
[22] E.L. Sjoberg, D.T. Rickard, Geochim. Cosmochim. Acta 48 (1984) 485.
[23] D.T. Rickard, E.L. Sjoberg, Am. J. Sci. 283 (1983) 815.
[24] C. Ludwig, W.H. Casey, J. Colloid Interface Sci. 178 (1996) 176.
[25] W.H. Casey, in: A. Hubbard (Ed.), Encyclopedia of Surface and Colloid Science, Dekker, New York, 2002, pp. 1486–1495.
[26] W.H. Casey, J. Colloid Interface Sci. 146 (1991) 586.
[27] Y. Inada, A.H. Mohammed, H.H. Loeffler, S. Funahashi, Helv. Chim. Acta 88 (2005) 461.
[28] G. Furrer, W. Stumm, Geochim. Cosmochim. Acta 50 (1986) 1847.
[29] W. Stumm, R. Wollast, Rev. Geophys. 28 (1990) 53.
[30] L.N. Plummer, T.M.L. Wigley, D.L. Parkhurst, Am. J. Sci. 278 (1978) 179.
[31] P. Van Cappellen, L. Charlet, W. Stumm, P. Wersin, Geochim. Cosmochim. Acta 57 (1993) 3505.